Growth of Epithelial Organoids in a Defined Hydrogel.

Broguiere, Nicolas ; Isenmann, Luca ; Hirt, Christian ; Ringel, Till ; Placzek, Silja ; Cavalli, Emma ; Ringnalda, Femke ; Villiger, Lukas ; Züllig, Richard ; Lehmann, Roger ; Rogler, Gerhard ; Heim, Markus H ; Schüler, Julia ; Zenobi-Wong, Marcy ; Schwank, Gerald

Abstract: Epithelial organoids are simplified models of organs grown in vitro from embryonic and adult stem cells. They are widely used to study organ development and disease, and enable drug screening in patient-derived primary tissues. Current protocols, however, rely on animal- and tumor-derived basement membrane extract (BME) as a 3D scaffold, which limits possible applications in regenerative medicine. This prompted us to study how organoids interact with their matrix, and to develop a well-defined hydrogel that supports organoid generation and growth. It is found that soft fibrin matrices provide suitable physical support, and that naturally occurring Arg-Gly-Asp (RGD) adhesion domains on the scaffold, as well as supplementation with laminin-111, are key parameters required for robust organoid formation and expansion. The possibility to functionalize fibrin via factor XIII-mediated anchoring also allows to covalently link fluorescent nanoparticles to the matrix for 3D traction force microscopy. These measurements suggest that the morphogenesis of budding intestinal organoids results from internal pressure combined with higher cell contractility in the regions containing differentiated cells compared to the regions containing stem cells. Since the fibrin/laminin matrix supports long-term expansion of all tested murine and human epithelial organoids, this hydrogel can be widely used as a defined equivalent to BME.

DOI: https://doi.org/10.1002/adma.201801621

ADVANCED MATERIALS
www.advmat.de

Growth of Epithelial Organoids in a Defined Hydrogel

Nicolas Broguiere, Luca Isenmann, Christian Hirt, Till Ringel, Silja Placzek, Emma Cavalli, Femke Ringnalda, Lukas Villiger, Richard Züllig, Roger Lehmann, Gerhard Rogler, Markus H. Heim, Julia Schüler, Marcy Zenobi-Wong, and Gerald Schwank**

Epithelial organoids are simplified models of organs grown in vitro from embryonic and adult stem cells. They are widely used to study organ development and disease, and enable drug screening in patient-derived primary tissues. Current protocols, however, rely on animal- and tumor-derived basement membrane extract (BME) as a 3D scaffold, which limits possible applications in regenerative medicine. This prompted us to study how organoids interact with their matrix, and to develop a well-defined hydrogel that supports organoid generation and growth. It is found that soft fibrin matrices provide suitable physical support, and that naturally occurring Arg-Gly-Asp (RGD) adhesion domains on the scaffold, as well as supplementation with laminin-111, are key parameters required for robust organoid formation and expansion. The possibility to functionalize fibrin via factor XIII-mediated anchoring also allows to covalently link fluorescent nanoparticles to the matrix for 3D traction force microscopy. These measurements suggest that the morphogenesis of budding intestinal organoids results from internal pressure combined with higher cell contractility in the regions containing differentiated cells compared to the regions containing stem cells. Since the fibrin/laminin matrix supports long-term expansion of all tested murine and human epithelial organoids, this hydrogel can be widely used as a defined equivalent to BME.

Organoids are self-organizing cellular structures that are grown in vitro from pluripotent stem cells (PSCs) or multipotent tissue-resident adult stem cells (ASCs). They mimic various aspects and functions of the respective tissue, and therefore are valuable models to study organ development and human diseases.[1] In addition, organoids provide a valuable tissue source for diverse biomedical applications such as drug screening and toxicology studies,[2–7] and in combination with genome editing tools might open up avenues for ex vivo gene therapy approaches.[8,9]

One of the first established and best studied organoid systems are murine small intestinal organoids grown from tissue resident ASCs.[10] When embedded in tumor-derived basement membrane extract (BME) (provided as the commercial product Matrigel or CultrexBME2) and supplemented with growth factors that mimic the intestinal stem cell niche

N. Broguiere, E. Cavalli, Prof. M. Zenobi-Wong
Department of Health Sciences and Technology
ETH Zürich
Otto-Stern-Weg 7, 8093 Zürich, Switzerland
E-mail: marcy.zenobi@hest.ethz.ch

L. Isenmann, Dr. C. Hirt, T. Ringel, S. Placzek, F. Ringnalda, L. Villiger, Prof. G. Schwank
Institute of Molecular Health Sciences
ETH Zürich
Otto-Stern-Weg 7, 8093 Zürich, Switzerland
E-mail: gerald.schwank@biol.ethz.ch

Dr. R. Züllig, Prof. R. Lehmann
Division of Endocrinology
Diabetes and Clinical Nutrition
University Hospital
Zurich 8091, Switzerland

The ORCID identification number(s) for the author(s) of this article can be found under https://doi.org/10.1002/adma.201801621.

DOI: 10.1002/adma.201801621

Prof. G. Rogler
Department of Gastroenterology and Hepatology
University Hospital Zurich
University of Zurich
Zurich 8091, Switzerland

Prof. M. H. Heim
Department of Biomedicine
University Hospital Basel
University of Basel
Basel CH-4031, Switzerland

Prof. M. H. Heim
Division of Gastroenterology and Hepatology
University Hospital Basel
Basel CH-4031, Switzerland

Dr. J. Schüler
Charles River Research Services Germany GmbH
Am Flughafen 12, 79108 Freiburg im Breisgau, Germany

(R-spondin, noggin, EGF), single Lgr5 positive (Lgr5$^+$) stem cells grow into organoids. In a first phase they form spherical cysts that mainly consist of proliferating progenitor cells, and after ≈2–4 days they further transform into complex 3D structures with multiple outward-pointing buds. These crypt-like domains contain the cell types that normally reside in small intestinal crypts, including Lgr5$^+$ stem cells, and the core domain of the organoid mainly contains the cell types that normally line the villi of the intestinal epithelium.[10,11] Since organoids can be regrown after mechanical or enzymatic dissociation, the system allows rapid and seemingly indefinite expansion of intestinal stem cells and primary intestinal epithelium in vitro. Adaptations of the growth factor cocktail also allow the growth of epithelial organoids from various other murine and human tissues.[12]

The establishment of organoid culture protocols critically depended on the use of the 3D scaffold BME.[10,13–17] This hydrogel consists of a heterogeneous mixture of extracellular matrix (ECM) proteins, proteoglycans, and growth factors secreted from Engelbreth–Holm–Swarm murine sarcomas.[18] The xenogeneic components and batch-to-batch variations strongly limit the use of cells grown in this matrix for clinical applications such as regenerative medicine and high-content screening.[18–20] In addition, due to the heterogeneous composition, precise modulation of physical and biochemical properties is not possible.[21] Hence there is a strong interest in finding defined substitutes to BME, and recently researchers developed polyethylene glycol (PEG)-based gels that mimic some of the features of BME.[22,23]

Here we designed a defined fibrin-based hydrogel that supports long-term expansion of epithelial organoids derived from different mouse and human tissues. We characterized the required mechanical and biological properties of the hydrogel, and studied the forces that organoids exert on the matrix at different stages of their growth. Our findings provide insights into organoid morphogenesis and organoid–ECM interactions, and provide a basis for the development of clinical-grade organoid protocols for future applications in regenerative medicine.

In our attempt to generate a defined matrix for culturing organoids, we first searched for a hydrogel that fulfills the physical requirements to support organoid growth. For this purpose, we tested whether known well-defined and biocompatible matrices support organoid growth when supplemented with an amount of BME that is high enough to provide the required biological signals, but too low to provide significant mechanical support. We selected four different scaffolds that span a wide range of biological, physical, and chemical characteristics. A fully synthetic transglutaminase (TG) cross-linked and neutrally charged polyethylene glycol (PEG) gel,[24] a semisynthetic TG cross-linked and highly negatively charged hyaluronan (HA) gel,[25] a natural calcium cross-linked and highly negatively charged alginate gel,[26] and a human-derived thrombin cross-linked fibrin gel that harbors both positive and negative charges (overall pI 5.5).[27] Since we reasoned that organoids require space for their increase in size during growth, we generated either degradable or deformable versions of these hydrogels: the PEG and HA gels contained the matrix metalloproteinase (MMP) sensitive peptide sequence GPQGIWGQ[28,29] integrated in their cross-linker, the alginate gel was weakly cross-linked with a method known to enable cell infiltration despite insensitivity to protease degradation,[26,30] and fibrin hydrogels are inherently degradable by proteases.

The gelation protocols of the four different hydrogels were first fine-tuned in order to obtain rheological properties similar to BME (Figure S1, Supporting Information). We then performed an organoid formation assay (**Figure 1**A–D), and seeded a cell suspension of mouse small intestinal epithelial cells into the different hydrogels, with or without 10% v/v BME supplementation. The frequency of cyst formation from single intestinal stem cells after three days (colony formation efficiency) was equally high in the fibrin gel supplemented with 10% v/v BME as in pure BME. In fibrin alone as well as the other tested hydrogels, colony formation efficiencies were significantly lower. In addition, when the rounded cysts were allowed to grow for eight days in the fibrin/BME hydrogel, they formed the crypt-like budding structures that are typical for murine small intestinal organoids (Figure 1E). We therefore concluded that fibrin provides an appropriate physical support for organoid cultures, but that biological signaling from one or several of the BME components is necessary for proper growth.

To further optimize the physical properties of the fibrin-based hydrogel for intestinal organoid culturing, we next modulated the stiffness of the gel by varying the concentration of fibrin (**Figure 2**A). Using the colony formation assay, we found that fibrin concentrations between 1.5 and 6 mg mL^{-1}, which correspond to stiffness between 24 ± 10 Pa (SD, n = 6) and 270 ± 8 Pa (SD, n = 3), allowed efficient formation of round cysts (Figure 2B,F). Increasing the fibrin concentration to 7.5 mg mL^{-1}, which generates a hydrogel with a stiffness of 492 ± 78 Pa (SD, n = 3), led to the formation of dense spheroids that did not continue to grow into budding organoids. The lower fibrin concentration of 1.5 mg mL^{-1} on the other hand resulted in gel degradation already after four days, and therefore also impaired organoid expansion (Figure 2C). We conclude that fibrin hydrogels between 3 and 4.5 mg mL^{-1} (77 ± 25 Pa (SD, n = 3) and 140 ± 47 Pa (SD, n = 4)) provide the best physical properties for organoid expansion.

To further compare the physical properties of the fibrin-based hydrogel and BME, we measured the pore sizes of the two scaffolds. Since both matrices are protein based, we used fluorescein-succinimidyl ester (F-NHS) to fluorescently label their backbones and analyzed the microstructures by confocal imaging. Consistent with scanning electron microscopy analysis,[31,32] we found that while BME generates a dense network with pores smaller than the resolution limit (estimated around 200 nm with confocal imaging), fibrin generates a sparse web of thick fibers with a pore size of ≈4 µm (Figure 2E). Analysis of the fibrin-based hydrogel supplemented with 10% BME further demonstrates that the mixed hydrogel consists of a sparse network of fibrin fibers filled with a thin mesh of BME (Figure 2E).

A recently developed protocol that allows the expansion of intestinal stem cells in a functionalized PEG gel demonstrated that RGD motifs are required for intestinal stem cell proliferation.[22] As these domains occur naturally in fibrin, we speculated that integrin binding to RGD is also one of the key requirements for organoid growth in fibrin-based gels. To test this hypothesis, we performed the organoid formation assay with soluble RGD peptides as a competitive inhibitor to

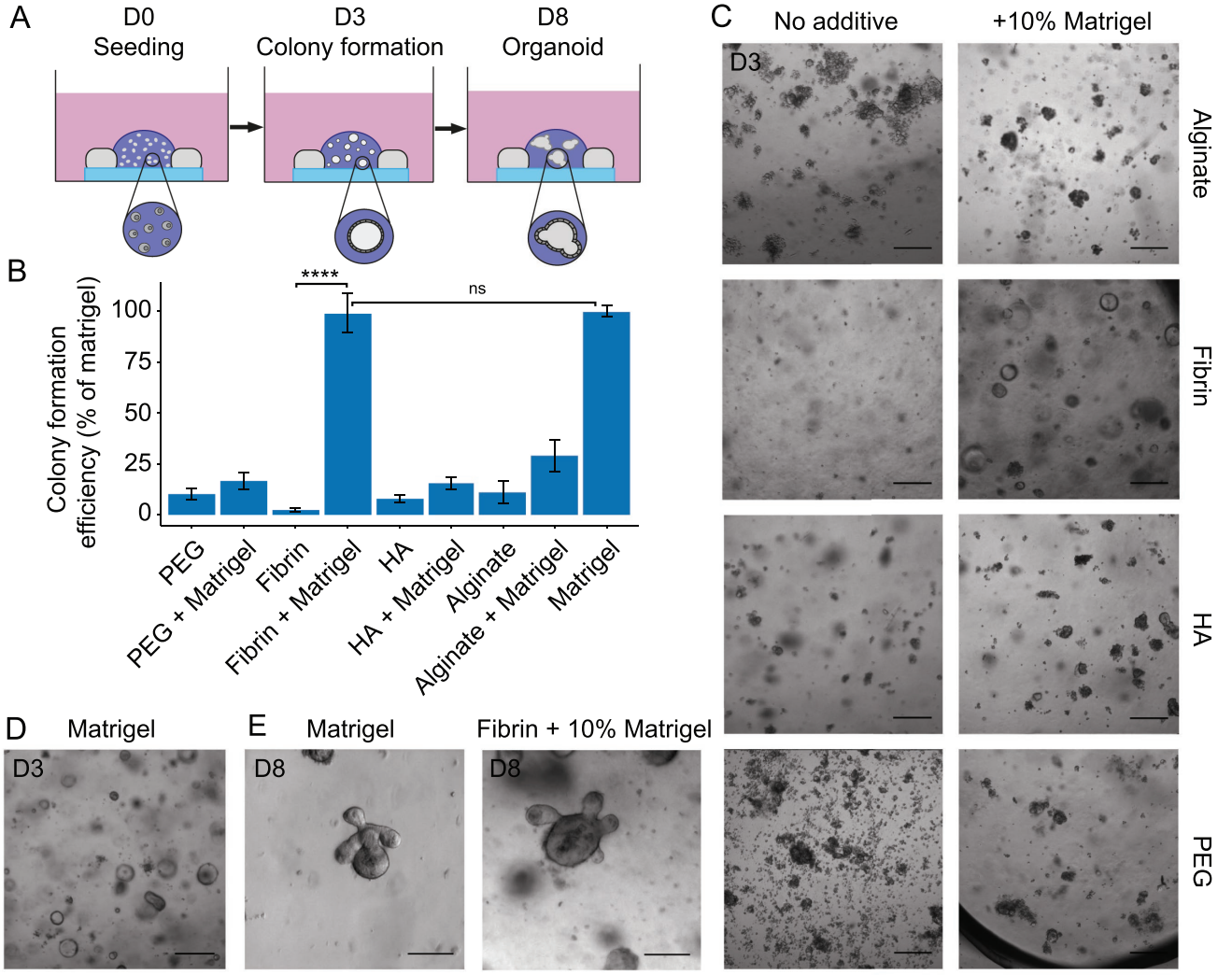

Figure 1. A) Scheme of seeding assay showing the hydrogel inside a silicone mold on a glass cover slip. Small intestinal stem cells first grow as cystic spheres as seen at day 3 (D3) followed by the formation of budding organoids after approximately one week. B) Quantifications of colony formation efficiency of mouse small intestinal stem cells in different hydrogel backbones with or without supplementation with 10% Matrigel. Data are expressed as a percentage of the colony count in Matrigel (100%). Error bars: SD, $n = 5$. C,D) Representative brightfield images of the cultures in the different hydrogels and Matrigel control. Scale bars: 200 µm. E) Budding organoids as seen in Matrigel and in fibrin + 10% Matrigel after 8 days. Scale bars: 100 µm.

extracellular matrix RGD binding (Figure 2D). We found that upon addition of soluble RGD organoid formation was inhibited, suggesting that RGD domains on the matrix are necessary for organoid growth. Of note, laminin, one of the main components of Matrigel, also contains RGD sites. However, while fibrin at 3 mg mL^{-1} provides a concentration of $\approx 35 \times 10^{-6}$ M,[33] 10% Matrigel only provides a concentration of $\approx 0.7 \times 10^{-6}$ M, which might be too low to provide a biological effect.

Finally, we asked if increasing RGD densities on the scaffold further enhances organoid growth. Via factor XIII-mediated anchoring we coupled additional RGD ligands to the 3 mg mL^{-1} fibrin matrix, while keeping its mechanical properties constant. We found that doubling or tripling the RGD densities neither affected the colony number nor the organoid morphology, suggesting that the natural RGD concentration on fibrin is sufficient for optimally promoting organoid growth (Figure S2, Supporting Information).

The dependency of organoid growth on RGD binding sites on the scaffold prompted us to investigate the mechanical forces that organoids exert on the matrix. After stem cell seeding, when organoids form spherical cysts, they are thought to adapt this shape by building up internal pressure via ion channel-mediated fluid influx.[34] Whether organoids form buds because the crypt-like structures pull on the matrix to protrude out of the organoid core (invasive collective cell migration), or because the organoid core becomes more contractile and as a consequence the internal hydrostatic pressure pushes the buds out (spatial differences in contractility), is however not known.[35] To answer this question, we analyzed the force distribution of growing organoids in the fibrin-based hydrogel with 3D traction force microscopy. We therefore tagged the fibrin matrix with TG modified fluorescent polystyrene nanoparticles, which anchor to fibrin during gelation and allow tracking of gel deformations. In our experimental setup,

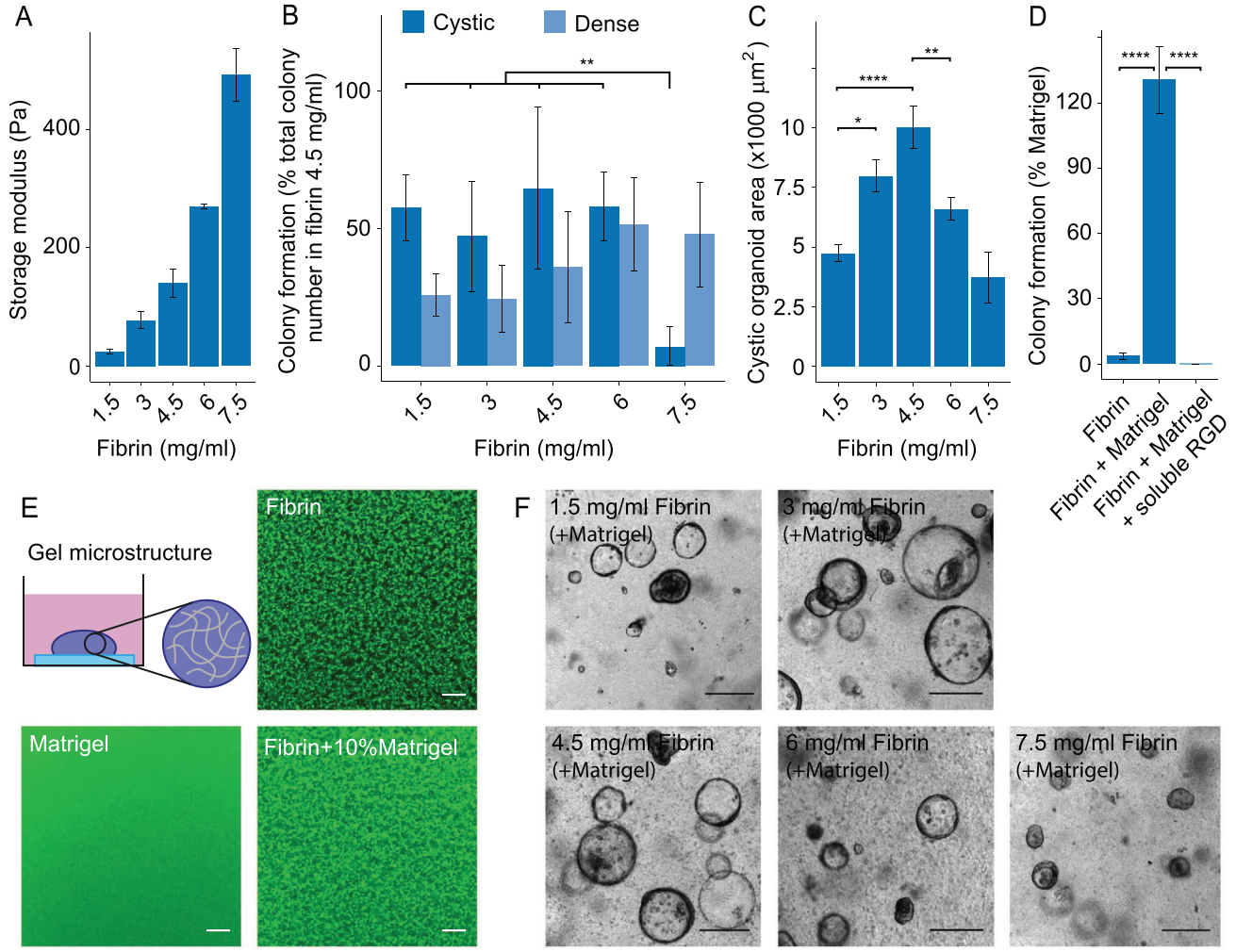

Figure 2. A) Storage Modulus of fibrin hydrogels with different fibrin concentrations. Error bars: SD, $n = 3$. B) Number of cystic or dense mouse small intestinal organoids four days after seeding in fibrin gels of different stiffness supplemented with 10% Matrigel. Error bars: SD, $n = 6$. C) Size of cystic organoids four days after seeding in different concentrations of fibrin gels supplemented with 10% Matrigel. Error bars: SEM $n = 67/65/74/66/3$. D) Effect of soluble RGD peptides on the colony formation efficiency of mouse small intestinal stem cells in fibrin-based hydrogels (3 mg mL^{-1} fibrin + 10% Matrigel). Error bars: SD, $n = 4$. E) FITC staining of Matrigel, Fibrin gels and Fibrin gels supplemented with 10% Matrigel showing the different microstructures. Scale bars: 20 µm. F) Representative brightfield images of mouse small intestinal organoids in fibrin gels of different stiffnesses after four days. Scale bar: 100 µm.

we first imaged the organoid during growth, then killed the organoid by adding sodium azide to the medium to relax the active cell forces, and finally imaged the same position again. Custom Matlab scripts (link provided in the Experimental Section) were subsequently used to track the matrix deformations in 3D and to reconstruct the cellular forces. Since we used the equations of mechanics for linear elastic materials under small deformations, which are only valid as a first approximation, our results should be considered an estimate rather than a quantitative measurement of the cell forces.

We observed that rounded cystic organoids initially developing from intestinal stem cells typically exerted a nearly spherical pressure on their matrix, consistent with expected active fluid uptake through ion pumping (**Figure 3**A). After initial cystic expansion, mouse small intestinal organoids start to form villus-like structures that mimic the in vivo architecture of the small intestinal epithelium. Interestingly, when we analyzed the forces generated by these asymmetrically growing organoids, we observed that the organoids still push on the matrix at the crypt-like domains, but start to pull on the gel around the central lumen (core domain) (Figure 3B,C). Since intestinal stem cells reside in the crypt-like domains of the organoids,[10] and since stem-cell rich early cystic organoids usually adopt a spherical morphology, our measurements suggest that the morphogenesis of budding organoids is due to the presence of differentiated cells with higher contractility. This results in the invagination of the core domain, and outward protrusion of the less contractile stem-cell rich areas under the influence of internal pressure.

Cell contractility is usually mediated by the actin cytoskeleton and molecular motors.[35] We therefore searched for an independent confirmation of this hypothesis by looking at F-actin

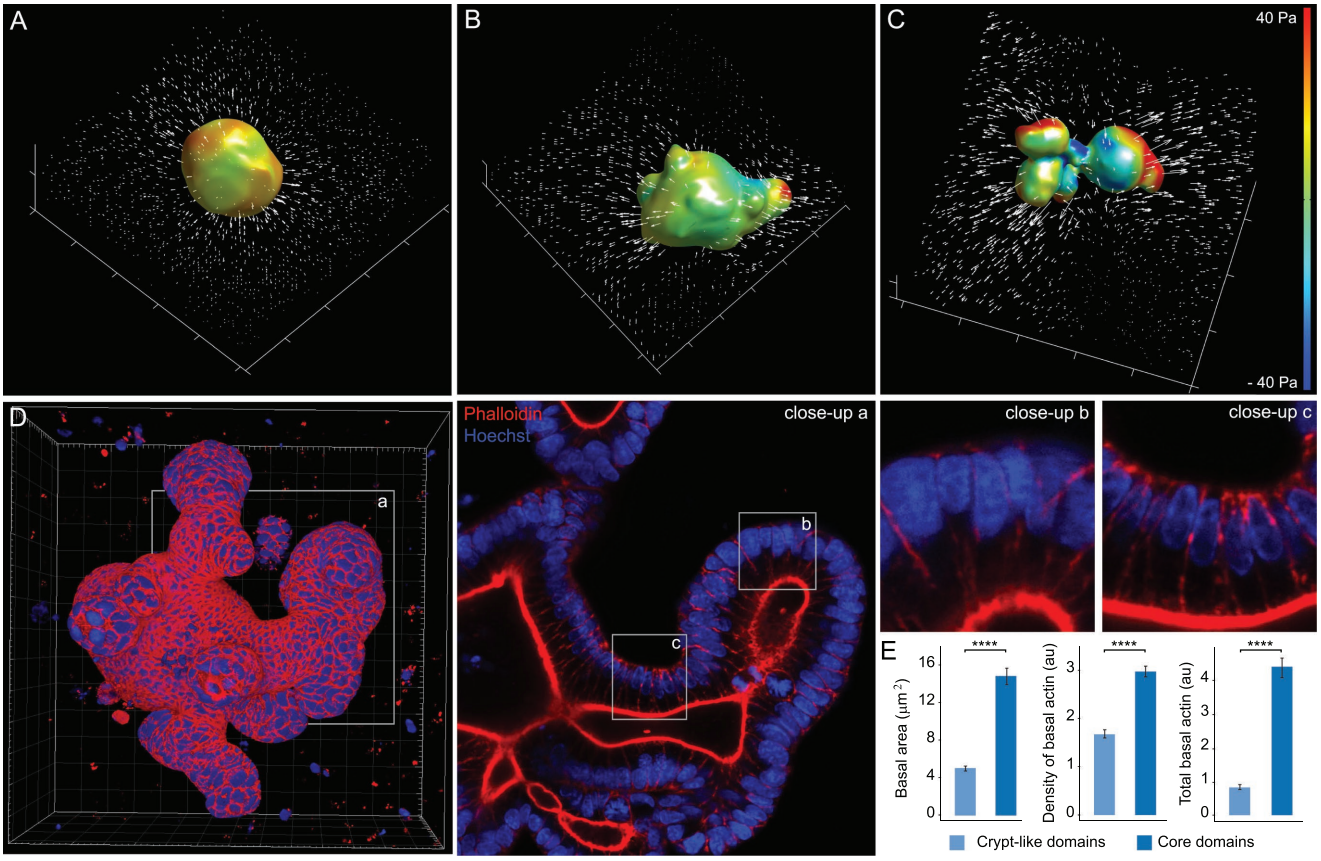

Figure 3. A–C) Representative 3D traction force microscopy measurements of a cystic, an early budding and a late budding organoid (from left to right). Normal pressures (i.e., normal vector * stress tensor * normal vector) are color-displayed on the surface of the segmented organoids, and the white arrows are the local displacements of the matrix amplified threefold. Gradations on the bounding box are 100 µm. D) Surface view of a representative late budding organoid stained with phalloidin (actin) and Hoechst (nuclei) using Imaris software, with single-plane close-ups of the marked areas, highlighting basal actin machinery in the core-like domains but not the cyst-like domains. Main gradations on the bounding box are 40 µm. E) Quantification of the surface area between the nucleus and the basal membrane, as well as the density and total amount of F-actin in this area (basal actin), for cells located in crypt-like domains (as shown in close-up (b)) or core domains (as shown in close-up (c)). Values are the averages ± SEM over 107 crypt cells and 128 core cells from five different organoids, with only cells lying horizontal in the imaging plane used for quantification.

distribution in budding organoids. 3D surface views and single plane close-up views showed that cells in the core regions but not in the crypt-like regions contained a shell of basal actin, between the nucleus and the outer membrane (Figure 3D). On the apical side, there was little to no cytoplasmic F-actin in either region, except for the well-known dense F-actin pillars supporting the microvilli. This pattern appeared consistently on all imaged organoids, and resulted in a large quantitative difference of basal actin distribution between core domains and cyst-like domains of organoids (Figure 3E).

We next aimed to identify the component of BME that provides the biological signals required for organoid growth in the fibrin matrix. We therefore supplemented the fibrin hydrogel with the main ECM components of BME: collagen IV, heparin (a glycosaminoglycan that mimics heparan sulfate proteoglycans), and the laminin-111/entactin complex (hereinafter referred to as laminin). To compensate for a potential loss of functionality of the purified components, we generated hydrogels with a final concentration of the additives at least twice as high as in 10% BME. The heparin was modified chemically to be TG cross-linkable, in order to ensure retention in the fibrin gels. Laminin and collagen IV are large proteins known to self-assemble into an insoluble matrix in physiological conditions and were therefore kept unmodified. While neither supplementation with collagen IV nor with heparin supported organoid formation in our assay, the colony formation efficiency in fibrin gels supplemented with laminin was comparable to that in pure BME ($p = 0.15$) (**Figure 4**A,B). In addition, when allowed to grow for longer periods, organoids also formed the crypt-like structures that are typical for murine small intestinal organoids (**Figure 5**A). To further identify the optimal laminin concentration for organoid formation and growth, we next performed the colony formation assay with fibrin gels supplemented with different amounts of laminin. While laminin concentrations of 0.5 mg mL^{-1} already led to stem cell proliferation and formation of rounded cysts, further increasing the concentrations enhanced the colony formation efficiencies. At 2 mg mL^{-1}, the organoid formation efficiency and phenotype were similar to pure BME (Figure 4C; Figure S3, Supporting Information).

To next assess if small intestinal organoid colonies in fibrin/laminin gels grow from $Lgr5^+$ stem cells, we isolated green fluorescent protein (GFP) positive cells from an organoid line that contains a Lgr5-GFP reporter by FACS, and seeded them

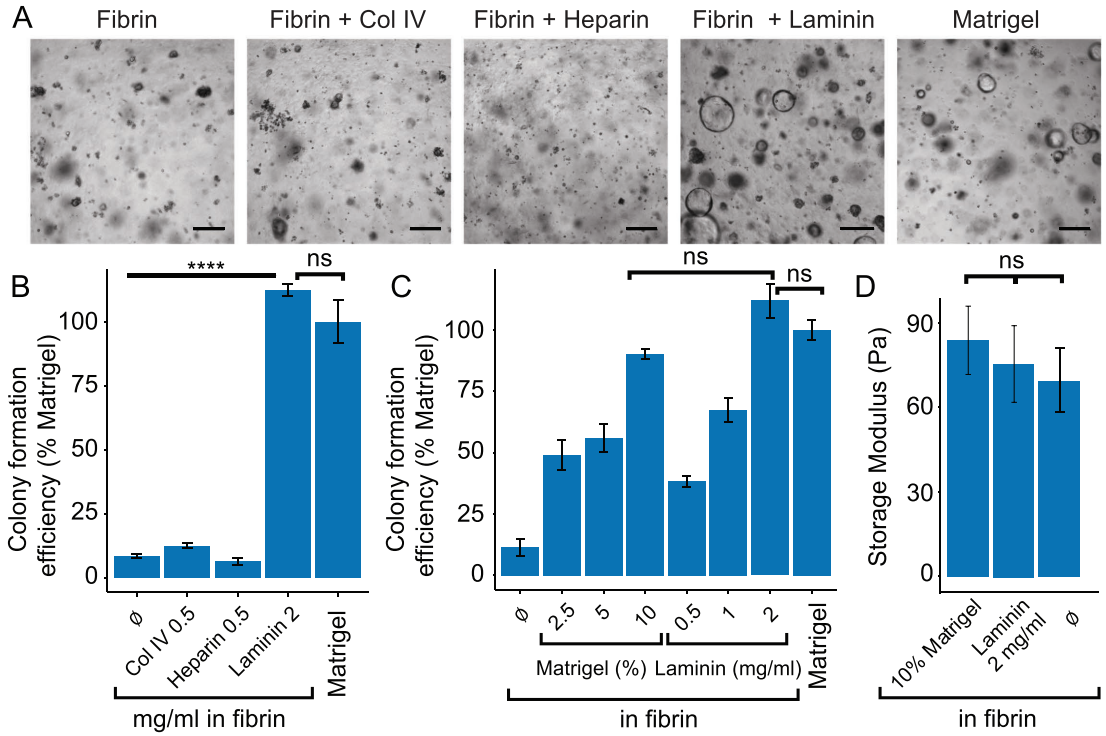

Figure 4. A) Mouse small intestinal stem cells four days after seeding in fibrin based hydrogels supplemented with Collagen IV, Heparin, Laminin, or in pure Matrigel. Morphology in brightfield microscopy. Scale bars: 200 µm. B) Quantification of the colony formation efficiency normalized to the Matrigel control. Error bars: SD, $n = 4$. C) Colony formation efficiency of mouse small intestinal stem cells seeded in fibrin gels supplemented with varying amounts of laminin or Matrigel. Error bars: SD, $n = 6$. D) Quantification of the changes in mechanical properties associated with the addition of Matrigel or laminin to fibrin hydrogels (3 mg mL^{-1}), as measured by rheometry. Error bars: SD, $n = 3$.

into the hydrogel. Like in BME, individual GFP positive cells formed clusters, which further developed into cystic organoids (Figure S4, Supporting Information). Finally, we also investigated if organoid lines can be directly established in fibrin/laminin gels from small intestinal crypts. Crypts were freshly isolated from Lgr5-GFP mice, and seeded into fibrin/laminin. Importantly, the organoid formation from isolated crypts was comparable to BME (Figure S5, Supporting Information).

To test if the defined fibrin/laminin hydrogel supports long-term expansion of murine small intestinal organoids, we passaged organoids in the gel for more than two months (>12 passages). Like organoids grown in pure BME, organoids grown in fibrin/laminin maintained their typical architecture, with crypt-like structures pointing outwards from the central lumen (Figure 5A). These organoids were also positive for the epithelial cell marker E-cadherin, contained $Lgr5^+$ stem cells and Paneth cells in the crypt-like domains, and had goblet and enteroendocrine cells scattered throughout the organoid structure (Figure 5A). To test whether the fibrin/laminin hydrogel is also applicable to other types of epithelial organoid cultures, we cultured human organoid lines derived from the small intestinal epithelium, liver, pancreas, and pancreatic ductal adenocarcinoma (PDAC) (Figure 5B). Of note, since human laminin shares 96% homology with mouse laminin (from UniProt sequence alignment), we used murine laminin also for expanding human organoid cultures. The phenotype of human liver and pancreas organoids was analyzed by immunocytochemistry, and like those grown in BME, expressed the ductal marker cytokeratin-19 (CK19) and progenitor marker SOX-9 (Figure 5C; Figure S6, Supporting Information). Organoids, moreover, expressed the epithelial markers E-cadherin and β-catenin, as well as the marker Ki-67, demonstrating that the cells were in a proliferative state (Figure S6, Supporting Information). In addition, gene expression levels of pancreatic and liver organoid specific markers were quantified by qPCR, and no difference was observed between organoids grown in BME and fibrin/laminin (Figure S7, Supporting Information). To further test for functional differences between organoids grown in the different hydrogels, we performed a drug assay with the pancreatic cancer drugs gemcitabine and paclitaxel on pancreatic and PDAC organoids grown either in pure BME, fibrin + 10% BME or fibrin/laminin. Again, no significant difference could be observed between organoids grown in the different hydrogels (Figure S8, Supporting Information). Importantly, all tested human organoid lines could also be expanded and passaged repeatedly in the fibrin/laminin hydrogel (>6 passages tested for each line), suggesting that fibrin/laminin could be used as a universal alternative to BME for culturing organoids derived from different types of tissues.

Here we studied in detail how mouse small intestinal organoids interact with their matrix, and used the data to establish a well-defined hydrogel that supports the long-term expansion of organoids derived from different mouse and human epithelial tissues. We found that fibrin is a suitable scaffold that could

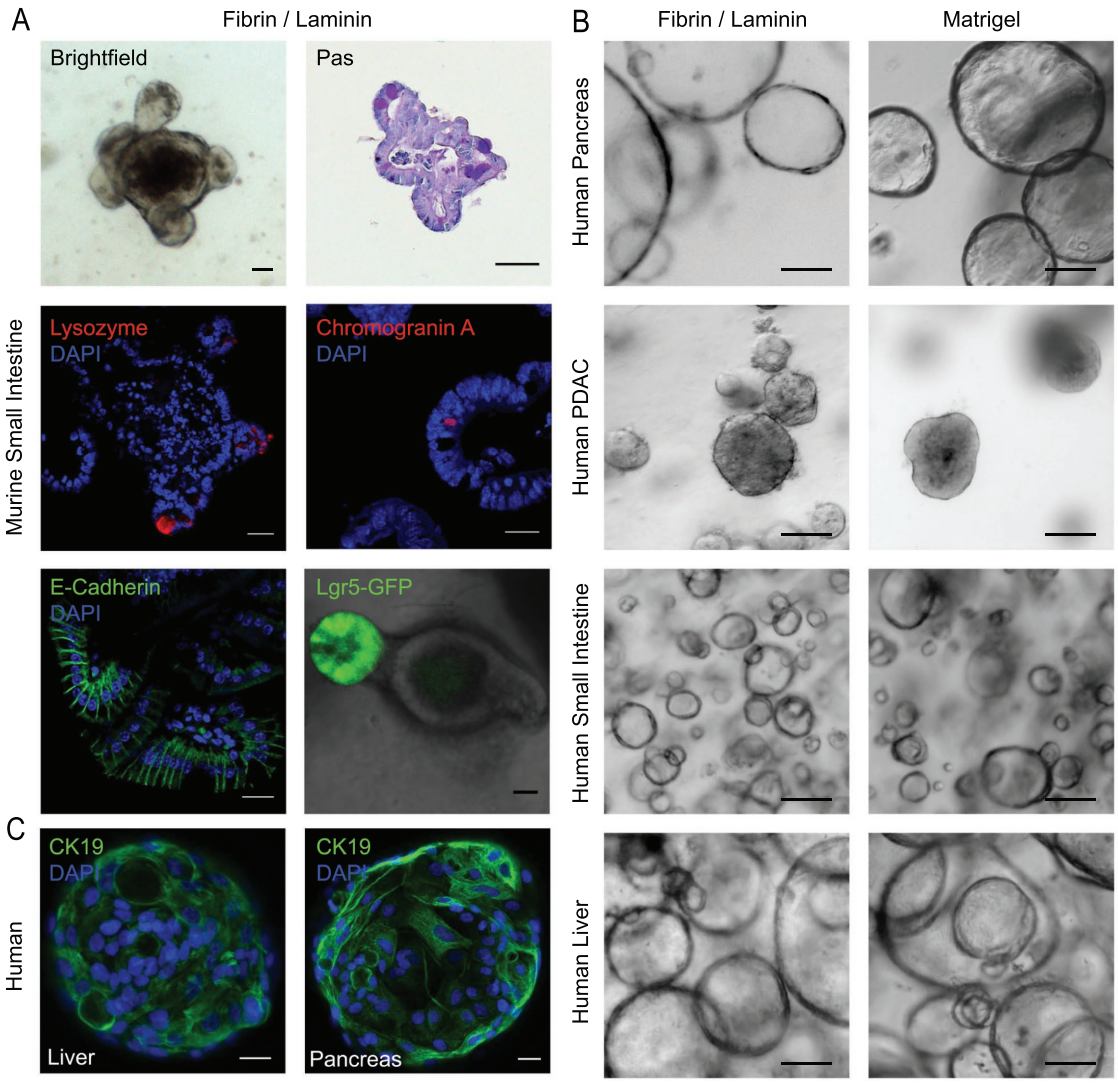

Figure 5. A) Mouse small intestinal organoids cultured long term in fibrin hydrogels supplemented with 2 mg ml^{-1} laminin. The organoids were stained for Goblet cells (PAS), Paneth cells (lysozyme), enteroendocrine cells (Chromogranin A), epithelial cells (E-Cadherin), and stem cells (Lgr5-GFP). Lgr5-positive and lysozyme positive cells were mostly observed in crypt-like domains. PAS and chromogranin positive were scattered throughout the organoids. The majority of organoids contained cells positive for the first three cell markers, whereas organoids containing chromogranin positive cells were less frequently observed. B) Various types of human epithelial organoids cultured > 6 passages in the fibrin/laminin hydrogels (left panel) and in Matrigel (right panel): human pancreas organoids, human pancreatic ductal adenocarcinoma organoids, human small intestinal organoids, and human liver organoids. C) Immunocytochemistry on human pancreas and liver organoids showing expression of the ductal marker cytokeratin 19 (CK19). Scale bars A: 20 µm, B: 100 µm, C: 20 µm.

act as a physical substitute for BME. The mechanical as well as biochemical properties of the fibrin matrix are important parameters for organoid expansion, as increasing the stiffness of the gel or blocking the RGD domains in the scaffold inhibited growth. We further found that the transition from spherical organoids to budding organoids was associated with a shift of force distribution exerted on the matrix: while cystic organoids applied uniform pressure on the matrix, in differentiated organoids pushing forces became predominantly restricted to the crypt-like domains and the core domains counteracted the internal pressure with increased contractility. Finally, we identified laminin as the major biological signaling molecule in BME that is required for organoid growth.

To our knowledge, the here developed fibrin/laminin hydrogel is the first well-defined 3D matrix that allows long-term expansion of organoids containing both progenitor and differentiated cells. Recently, two independent studies described functionalized PEG-based hydrogels that also support the growth of intestinal progenitor cells in 3D in vitro.[22,23] Compared to BME, synthetic PEG hydrogels, however, have certain disadvantages. Gjorevski et al. reported the necessity of two different PEG hydrogels for intestinal organoid growth: a stiff nondegradable PEG gel that promotes intestinal stem cell expansion as spheroids, and a soft and hydrolyzing PEG gel that constrains stem cell proliferation but triggers differentiation into the functional cell types of the intestinal epithelium.

The PEG-based hydrogel described by Cruz-Acuña et al. required initial expansion of pluripotent progenitor cells in 2D cultures on a layer of BME, and differentiation of 3D spheroids into functional intestinal epithelial cells was only demonstrated after in vivo transplantation into mice. In addition, the expansion of human pluripotent stem cell-derived spheroids[23] required very different physical properties than the expansion of murine adult stem cell derived spheroids,[22] indicating that each PEG hydrogel formulation is limited to a narrow range of applicability. Indeed, when we reproduced the PEG hydrogel described by Cruz-Acuña et al., we found that it enabled growth of human liver and pancreas organoids, but did not support expansion of murine small intestinal organoids. The morphology of human liver and pancreas organoids was moreover different than when grown in BME and fibrin/laminin (Figure S9, Supporting Information). Taken together, our data suggests that the fibrin/laminin gel has a broader range of applicability, and could be widely used to substitute BME for culturing organoids derived from different tissues.

The development of a defined fibrin-based hydrogel for organoid growth opens novel possibilities for studying complex tissues in 3D in vitro. For example, the fibrin sites for factor XIII mediated covalent anchoring,[36] which we used here to couple fluorescent nanoparticles for 3D traction force microscopy, could also be used to directly anchor specific peptides or biomolecules, and to study their influence on cellular mechanisms. In addition, the fibrin matrix could offer several advantages for high-content drug screening in organoids compared to BME. First, it is relatively inexpensive, and using fibrin supplemented with 10% BME instead of pure BME would therefore significantly reduce the costs of an organoid screening platform. Second, enzymatic gelation of fibrin offers advantages over the thermoresponsive BME, as it does not require cooling of the liquid-handling robots. Finally, by demonstrating a crucial role of laminin for organoid expansion, our work encourages the development of clinical-grade laminin, or laminin-subdomains that mimic its signaling function.[37] The latter might be necessary, as laminin is a large protein complex prone to self-polymerization, making its production and purification particularly challenging. Importantly, since human fibrin is already commonly used as a tissue sealant in surgeries, these hydrogels could pave the way for the use of organoids in regenerative medicine to replace diseased epithelial tissues in patients with in vitro grown organoid epithelia.

Experimental Section

Mouse Tissues: All animal experiments were performed in accordance with protocols approved by the Kantonales Veterinäramt Zürich. Following mouse lines were used in this study: Lgr5-EGFP-IRES-creERT2 (JAX 008875), CAG-eGFP (JAX 006567), C57BL/6J (JAX 000664).

Human Tissues: Human liver biopsies (ultrasound-guided needle biopsies) were obtained from the University Hospital Basel, human intestinal biopsies were obtained from the University Hospital Zürich, human pancreatic tissue was obtained from pancreatic islet isolation procedures from the University Hospital Zürich, human PDAC tissue was obtained from a previously established patient-derived xenograft (PDX) mouse model (Charles River Research Services Germany GmbH). Written informed consent was obtained from all patients, and the study was approved by the Cantonal Ethics committee of the north-western part of Switzerland and the Cantonal Ethics Committee of the Canton Zürich.

Organoid Isolation and Culturing: Mouse small intestinal organoids were isolated as previously described.[10] In short, the mouse small intestines was removed and flushed several times with phosphate buffered saline (PBS, Gibco, pH7.4). The small intestine was then placed in cold PBS, opened up longitudinally, and the villi were scraped off using a glass microscope slide. The intestine was cut into 2–4 mm pieces and transferred into a 50 mL tube containing 10 mL of PBS. Subsequently the pieces were pipetted up and down and PBS replaced several times until the supernatant was clear. The supernatant was removed and the intestine pieces incubated in 25 mL of 2×10^{-3} M ethylenediaminetetraacetic acid (EDTA) in PBS on ice for 60 min. The solution was pipetted up and down several times, pieces were transferred into 10 mL PBS containing 10% fetal bovine serum (FBS), and the tube was shaken vigorously. The suspension was passed through 70 µm cell strainer (BD Biosciences), and centrifuged at 150 g. The pellet was then resuspended in growth factor reduced (GFR) Matrigel (Corning—lot numbers: 5257008, 7030565, 261008) at a density of ≈50–100 crypts per 20 µL. The solution was plated in 20 µL drops on prewarmed standard tissue culture plates (Greiner Bio-one), and after gelation at 37 °C small intestinal organoid medium containing 10×10^{-6} M RhoKinase inhibitor (Y-27632, Abmole) was added. Mouse Small intestinal organoids were cultured at 37 °C in 5% CO_2 in Advanced Dulbecco's modified Eagle media (DMEM)/F12 (Gibco) supplemented with 10×10^{-3} M HEPES (Gibco), 1 × Glutamax (Gibco), 1% (or 100 U per mL) Penicillin/Streptomycin (Gibco), 1 × N2 (Gibco), 1 × B27 (Gibco), 1.25×10^{-3} M *N*-Acetylcysteine (Sigma), 5% in-house produced conditioned medium (CM) R-Spondin-1, 10% in-house produced CM Noggin, 50 ng mL^{-1} human EGF (Peprotech). Organoids were passaged either by mechanical dissociation using a fire-polished Pasteur pipette, or by incubation in TrypLE Express Enzyme (1x) (Gibco) for 10 min.

Human intestinal organoids were established from patient biopsies as described in van Wetering et al.[38] In short, the biopsies were placed in complete chelating solution (CCS) (5.6×10^{-3} M Na_2HPO_4, 8×10^{-3} M KH_2PO_4, 96.2×10^{-3} M NaCl, 1.6×10^{-3} M KCl, 43.4×10^{-3} M sucrose, and 54.9×10^{-3} M D-sorbitol). Dithiotreitol was added just before use to a final concentration of 0.5×10^{-3} M), as well as 2×10^{-3} M EDTA. The biopsies were then incubated for 20–45 min at 4 °C on a rocking plate. After incubation, tubes were shaken vigorously to liberate the crypts. Tissue fragments were allowed to settle for 1 min, and supernatant containing crypts was transferred to a new tube. One volume of FBS was added and crypts were spun down at 150 g for 3 min. Next, the crypts were washed twice with Advanced DMEM/F12 supplemented with 10×10^{-3} M HEPES, 1x Glutamax, 1% Penicillin/Streptomycin and finally spun down for 5 min at 150 g. The pellet was subsequently resuspended in GFR Matrigel, and plated in 20 µL drops on prewarmed standard tissue culture plates. After solidification of Matrigel, human small intestinal organoid medium containing 10×10^{-6} M RhoKinase inhibitor and 100 µg mL^{-1} Primocin (Invivogen) was added. Human small intestinal organoids were cultured in Advanced DMEM/F12 supplemented with 10×10^{-3} M HEPES, 1x Glutamax, 1% Penicillin/Streptomycin, 1x B27, 1.25×10^{-3} M *N*-acetylcysteine, 50% Wnt3a CM (produced in-house), 20% R-spondin-1 CM, 10% noggin CM, 10×10^{-3} M nicotinamide (Sigma), 50 ng mL^{-1} human EGF, 10×10^{-9} M Gastrin (Tocris Bioscience), 0.5×10^{-6} M A83-01 (Tocris Bioscience) and 10×10^{-6} M SB202190 (Sigma).

Human liver organoids were established from patient biopsies as described in Broutier et al.[39] Briefly, the biopsies were minced into pieces of roughly 0.5–1 mm and incubated in DMEM (Gibco) containing 2.5 mg mL^{-1} collagenase D (Roche) and 0.1 mg mL^{-1} DNase I (Sigma) for 20–60 min at 37 °C on a shaker. The digestion was stopped by adding two volumes of ice cold DMEM containing 10% FBS and 1% Penicillin/Streptomycin. Solution was filtered through a 70 µm nylon cell strainer. Residual liver was digested for 10 min with Accutase (Gibco) at 37 °C in the water-bath. Filtered solution was pelleted by 120 g centrifugation and resuspended in GFR Matrigel. Solution was plated in 20 µL drops on prewarmed standard tissue culture plates, and after gelation human

liver organoid medium containing 10×10^{-6} M RhoKinase inhibitor, 30% Wnt3a CM, and 10% Noggin CM was added. Human liver organoids were cultured in Advanced DMEM/F12 supplemented with 10×10^{-3} M HEPES, 1x Glutamax, 1% Penicillin/Streptomycin, 1x B27 without vitamin A (Gibco), 1x N2, 1.25×10^{-3} M *N*-acetylcysteine, 10×10^{-3} M nicotinamide, 50 ng mL^{-1} human EGF, 100 ng mL^{-1} FGF10 (Peprotech), 25 ng mL^{-1} HGF (Peprotech), 10×10^{-9} M gastrin, 5×10^{-6} M A83-01, 10×10^{-9} M prostaglandin E2 (Tocris Bioscience), 10×10^{-6} M forskolin (Tocris Bioscience), 10% R-Spondin-1 CM. Of note, noggin CM, Wnt3a CM, and RhoKinase inhibitor were only required in the first 3–4 days after the isolation.

Human pancreatic organoids were established from adult islet-depleted pancreatic tissue[35] obtained from islet transplant programs. Briefly, pancreatic tissue was hand-picked to assure that no islets would be subcultured. Small clumps of pancreatic cells were obtained by mechanical dissociation of the islet-depleted pancreatic tissue with a fire-polished Pasteur pipette. After three washes with ice-cold PBS, the clumps were allowed to settle for 3 min on ice. The last washing step was carried out in cold Advanced DMEM/F12. The supernatant was removed and the clumps were embedded in 30–40 µL drops of GFR Matrigel at a density of ≈15–20 clumps in prewarmed standard 24-well tissue culture plates. After GFR Matrigel had solidified, human pancreas organoid medium with additional 10×10^{-6} M RhoKinase inhibitor and 100 µg mL^{-1} Primocin (Invivogen) was added. The PDAC organoid line was derived from a previously established PDX PDAC line, which was obtained as single cell suspension, resuspended in Matrigel, and plated as 20 µL drops. Human Pancreas and human PDAC organoids were cultured in Advanced DMEM supplemented with 10×10^{-3} M HEPES, 1x Glutamax, 1% Penicillin/Streptomycin, 1x N2, 1x B27, 1.25×10^{-3} M *N*-acetylcysteine, 50% Wnt3a CM, 10% R-spondin-1 CM, 10% noggin CM, 10×10^{-3} M nicotinamide, 50 ng mL^{-1} EGF, 10×10^{-9} M gastrin, 100 ng mL^{-1} FGF10 and 0.5×10^{-6} M A83-01. Wild type pancreatic organoid medium was additionally substituted with 1×10^{-6} M prostaglandin E2.

Synthesis of Gel Precursors: FXIIIa cross-linkable PEG and HA were synthesized as described previously.[24,25] The protocol developed for HA modification with ≈10% substitution rate was applied to heparin, which is essentially identical in terms of chemical functionality, to obtain FXIIIa cross-linkable heparin. In short, 100 mg (0.168 mmol of the disaccharide repeat unit) of heparin (Sigma) and 5.95 mg (0.025 mmol) of 3,3′-dithiobis(propanoic dihydrazide) (DTPHY, Frontier Scientific) were dissolved in 10 mL of MES hydrate 150×10^{-3} M solution (resulting pH ≈4.2). Then 9.6 mg (0.05 mmol) of 1-ethyl-3-(3-dimethylaminopropyl) carbodiimide were prediluted in 0.5 mL of water and added dropwise over stirring. The reaction was left to proceed for 6 h at room temperature and without stirring. Then the disulfides were reduced overnight in a closed flask by addition of 34.5 mg (0.15 mmol) of tricarboxyethylphosphine (TCEP-HCl, Fluorochem), prediluted in 0.5 mL of water. The product was supplemented with 1 g of NaCl, and dialyzed against ultrapure water. After recovery, the dialyzate was added dropwise over stirring to 0.25 mL (2.5 mmol) of divinylsulfone (DVS) prediluted in 5 mL of triethanolamine buffer, 300×10^{-3} M, pH 8.0. Divinylsulfone is lethal in contact with skin and should be handled with special care. The reaction was left to proceed overnight at room temperature without stirring. Then 1 g of NaCl was added and the product was dialyzed against ultrapure water again. Finally, 62 mg of glutamine donor peptides (sequence NQEQVSPLERCG, amidified carboxyterminus) were added, and the product was again dialyzed against diluted NaCl followed by ultrapure water, and lyophilized. To confirm successful conjugation of the modified heparin to fibrin gels, a fluorescein derivative was also synthesized by reacting the previous compound with 1/100th equivalents fluorescein isothiocyanate (FITC) over the disaccharide repeat unit (which is ≈1/10th over the peptides, which provide free amino groups for conjugation at their aminoterminus). The conjugation was done in sodium hydrogen carbonate buffer, 100×10^{-3} M, pH 9.5, for 5 h at room temperature, and the product dialyzed and lyophilized.

Fibrin Gelation: Organoids were resuspended in 3 mg mL^{-1} fibrinogen (Tisseel, Baxter) and 0.1% nanocellulose (Growdex, UPM) in PBS containing 0.9×10^{-3} M $CaCl_2$ and 0.49×10^{-3} M $MgCl_2$. Depending on the experiment, the suspension was supplemented with 10% v/v GFR Matrigel (Corning) or 0.5–2 mg mL^{-1} laminin (Corning #354259) or 0.5 mg mL^{-1} human collagen IV (Sigma) or FXIIIa-cross-linkable heparin. Polymerization was induced by the addition of 0.5 U per mL thrombin and left to proceed for 30 min at 37 °C in a humidified incubator before adding culture medium. Fibrinogen and thrombin were prewarmed to 37 °C before use, all other components were kept at 4 °C before adding. The nanofibrillar cellulose is biologically inert and was only used to increases the viscosity during gelation in order to avoid sedimentation of organoids. The cellulose was not included in traction force microscopy measurements to avoid creating mechanical inhomogeneities, instead the gels were flipped during gelation to avoid sedimentation. Individual gels were ≈20 µL in volume, and could be formed and cultured equally well either as droplets at the bottom of 24 well-plates (for expansion), of a glass bottom plates (for imaging from bottom), or in 4 mm diameter x 1 mm height PDMS (Sylgard 184) molds adsorbed on 10 mm diameter coverslips (for easier handling during incubations and transfers as well as for imaging from the top).

HA Gelation: Dissociated organoids were resuspended in a 0.4% w/v transglutaminase cross-linkable HA solution in a buffer consisting of Tris 50×10^{-3} M, $CaCl_2$ 50×10^{-3} M, glucose 100×10^{-3} M, pH 7.6. The solution was then supplemented with FXIIIa 10 U per mL from a 200 U per mL stock (Fibrogammin, CSL Behring), distributed in silicon molds and left to gel for 30 min at 37 °C. Where applicable, 10% of the buffer was replaced by Matrigel.

PEG Gelation: Dissociated organoids were resuspended in a 1.2% w/v solution of TG cross-linkable 40 kDa 8-arm-PEG, in a buffer consisting of Tris buffer 50×10^{-3} M, $CaCl_2$ 50×10^{-3} M, NaCl 50×10^{-3} M, with pH7.6 and supplemented last moment with 10 U per mL FXIIIa from a 200 U per mL stock. The solution was pipetted into silicon molds, and gelation was left to proceed for 30 min at 37 °C. Where applicable, 10% of the buffer was replaced by Matrigel.

Alginate Gelation: Dissociated organoids were resuspended in a 0.15% w/v alginate solution (Novamatrix, high viscous) in cell culture medium. The solution was added to silicon molds. Then, the gel cylinders were covered with a cellulose membrane pre-wetted with a 10×10^{-3} M calcium chloride solution in medium, and an additional 100 µL of calcium solution was added on top. The gelation was left to proceed for 1 h at 37°. Where applicable, 10% of the buffer was replaced by Matrigel.

Matrigel Gelation: Dissociated organoids were resuspended in Matrigel, plated in 20 µL drops or pipetted in silicon molds, and gelled at 37 °C for 10 min.

Quantification of Intestinal Stem Cell Colony Formation Efficiency: Organoids were digested for 5 min at 37 °C using TrypLE and resuspended in the different hydrogels in silicon molds. After 3 or 4 days (see figure legends) the whole gels were imaged in brightfield (Zeiss observer) and the number of growing organoids was quantified manually. When applicable, the organoids size was quantified using manual segmentation in Fiji.

Rheological Measurements: The storage moduli of the hydrogels were determined with small-strain oscillatory shear measurements on a Physica MCR 301 rheometer (Anton-Paar) using a 20 mm diameter parallel plate geometry. The gels were formed in situ and gelation monitored with 20 s steps using oscillations at 1 Hz and 5% strain. For Cultrex BME2, Matrigel, and laminin, which are thermoresponsive, the rheometer was precooled to 4 °C and the temperature was set to 37 °C after 3 min of measurement. For PEG, HA, fibrin, y, which are enzymatically cross-linked, the rheometer was prewarmed to 37 °C and the enzyme was added and mixed swiftly immediately before the measurement. For alginate, a 10 mm parallel plate geometry was used instead, and the calcium solution was added all around the precursor/probe immediately after starting the measurement. All buffers, polymers, and enzyme concentrations were the same as described above.

Immunohistochemistry of Intestinal Organoids: Organoids were fixed for 2 h with 4% paraformaldehyde and subsequently embedded into paraffin using standard protocols. 4 µm tissue sections were stained.

Primary antibodies used: E-cadherin (BD 610182, 1:1000), lysozyme (Dako, A009902, 1:1750), chromogranin A (Santa Cruz, SC-13090, 1:200). Secondary antibodies were used 1:1000: Thermo-Fisher Scientific, Donkey anti-Rabbit Alexa Fluor 568 (A10042), or Donkey anti-Mouse Alexa Fluor 488 (A21202). For periodic acid Schiff staining (Sigma-Aldrich, 395B-1KT) and H&E staining, standard protocols were used.

Immunocytochemistry of Pancreas and Liver Organoids: Organoids were fixed and permeabilized for 2 h with 4% paraformaldehyde and 0.1% triton-X100 in PBS, blocked with 5% bovine serum albumin (BSA) in PBS overnight. The gels were then broken down by gentle pipetting, and the gel fragments were re-embedded in fibrin at 6 mg mL^{-1} in 5 µL droplets on a glass bottom 96 well plate. All the antibody incubations and PBS washes were done overnight. Antibodies, diluted in 5% BSA solution, were: E-cadherin (BD 610182, 1:1000), Ki67 (Abcam 15580, 1:300), CK-19 (Abcam 52625, 1:600), SOX-9 (Millipore 5535, 1:1000), HNF-4α (Santa-Cruz H-171, 1:1000), β-catenin (Abcam 32572, 1:200), goat anti-mouse IgG Alexa-594 (Invitrogen, 1:500), goat anti-rabbit IgG Alexa-488 (Invitrogen, 1:500).

RGD Competition Assay: Organoids dissociated with TrypLE and freshly plated in the applicable gels were incubated either in mouse small intestinal growth medium or small intestinal growth medium supplemented with 0.1×10^{-3} M RGD peptides (Anaspec, sequence Ac-GCGYGRGDSPG-NH2).

RGD Loading Assay: The method used was developed by Schense and Hubbell.[40] Factor XIIIa cross-linkable RGD-containing peptides with the sequence NQEQVSPLRGDSPG-NH2 were synthesized with classical solid-phase supported fmoc peptide synthesis on a Protein Technologies Prelude instrument and purified by reverse-phase (C18-silica) preparative high performance liquid chromatography (HPLC) on an Agilent Infinity 1260 instrument using a gradient of 10%–90% acetonitrile in water with 0.1% trifluoroacetic acid (TFA). Peptide identity was confirmed by mass-spectroscopy (1483 g mol^{-1}). The peptides were lyophilized, resuspended in ultrapure water, neutralized with dilute NaOH, sterilized by filtration at 0.2 µm, aliquoted and relyophilized for prolonged storage.

The peptides were mixed at 200 and 400×10^{-6} M from 2×10^{-3} M reconstituted PBS stocks in the fibrin 3 mg mL^{-1} + 10% Matrigel gels, and trypsinized mouse small intestinal organoid cells were encapsulated as described above. The medium was changed after 1, 3, and 12 h in order to wash unbound peptides, and the colony formation efficiency and morphology were observed after 4 d in culture from brightfield imaging (Zeiss Observer, 5x objective).

For peptide coupling quantifications, gels of 50 µL were formed in 200 µL tubes, as well as equivalent dilutions of peptides in PBS serving as standards. 50 µL of PBS was then added to each tube, and let the free peptide diffuse to equilibrium over 24 h. 10 µL of the solution was collected from each tube to analyze the percentage of free peptide in standards and in gel supernatants by analytical reverse-phase HPLC. The percentage of missing peptide (consistently found to be 14%–15%) was used to calculate the molarity of coupled RGD peptides.

The total amount of RGD peptides in the gels were calculated using reported values of two RGD sequences per fibrinogen alpha chain,[41] hence four RGD per fibrinogen 340 kDa hexamer. In Matrigel, RGD concentration was estimated using manufacturer's reported values of 9 mg mL^{-1} solid content including 60% of the 800 kDa laminin, which has one RGD site.

Hydrogel Microstructure Imaging: 15 µL hydrogel drops were placed in silicone molds on coverslips and gelled as described previously. After gelation, the hydrogels were covered with Advanced DMEM (Gibco) supplemented with 10×10^{-3} M HEPES, and incubated at 37 °C for 16 h. The gels were then washed three times for 20 min with PBS, and incubated with F-NHS (Thermo 46410) in PBS (1:120 dilution of a 1% w/v frozen stock in DMSO) for 2 h and finally washed 3×30 min with PBS. The hydrogels were imaged on a Leica TCS SP8 confocal microscope.

Fluorescent Nanoparticle Functionalization: 40 µL of 40 nm fluorescent polystyrene nanoparticle (nP) solution (Thermo F8793) was reacted in 100×10^{-3} M MES buffer, pH 4.5, with 40 µL of EDC 10×10^{-3} M and 40 µL of DTPHY 10×10^{-3} M. The reaction was left to proceed for 1 h. Then 1 mg of TCEP was added for reduction, which resulted in immediate nanoparticle precipitation. The particles could be redispersed by adding 500 µL of 1% sodium dodecyl sulfate (SDS) in water with sonication. The reaction byproducts were removed by repeated dilution in 1% SDS in water and reconcentration with a 100 kDa MWCO Vivaspin protein concentrator (2500 g, 10 min). 500 µL of nanoparticle suspension were recovered, and 10 µL of DVS prediluted in 500 µL of triethanolamine buffer, 300×10^{-3} M, pH 8.0, was added. The reaction was left to proceed for 10 min at RT, before washing and reconcentrating with the centrifugal filter. Finally, 2 mg of TG peptide NQEQVSPL-ERCG was dissolved in 500 µL of the triethanolamine buffer and added, left to react for 30 min at 37 °C, and the final TG-cross-linkable nanoparticles (nP-TG) product was isolated by washing first with tris buffered saline pH7.5 (TBS), and then with TBS + 0.1% BSA. The BSA was used here as a cytocompatible surfactant that can keep the modified nanoparticles in stable suspension. The resulting nP-TG stock was filtered at 0.2 µm and stored in the fridge for up to a few months.

Organoid Culture for Force Sensing Experiments: Mouse small intestinal organoids expressing GFP insert were dissociated with TrypLE and resuspended in a fibrin gels solution supplemented with Matrigel and modified with fluorescent nanoparticles (3 mg mL^{-1} Fibrin, 0.5 U per mL Thrombin, 10% to 40% v/v Matrigel, 0.5 U per mL thrombin, 5% v/v nP-TG stock, in calcium containing PBS). Eight well glass bottom plates (Ibidi µ-Slide) were prepared by placing a single silicone mold in each well. 15 µL of the organoid/hydrogel suspension were placed in each mold and incubated for 30 min at 37 °C. Subsequently, full mouse small intestinal growth medium was added and the cells incubated at 37 °C, 5% CO_2 for 1–5 days.

3D Traction Force Microscopy: The organoids were live-imaged with a 40 x water immersion objective and a white light laser providing simultaneous excitation at 488 and 594 nm, on a Leica SP8 confocal microscope equipped with CO_2 and prewarmed to 37 °C for typically 12 h (to stabilize from temperature-induced drifting). 0.2% sodium azide was added to the media from a 10% w/v stock, and the organoids were left to die for 2 h. The same positions were then imaged again as a relaxed reference.

The scripts used for force reconstruction from such images are provided on GitHub together with a user manual as well as extensively commented code (https://github.com/nbroguiere/TFM). No programming knowledge is needed to use this code, but basic understanding of mechanics and image analysis can be helpful in adjusting the parameters. In short, a cubic lattice was used with 10 µm spacing, and tracked the displacement of a 20 µm wide cubic box between the live and dead images on each position of this lattice using normalized cross-correlation with subpixel accuracy. Only normalized cross-correlation values above 0.7, which indicate a good match, were kept for further consideration. This provided an experimental displacement field. The organoids were also segmented from the GFP channel, and the position of the organoid was used to define the borders for the mechanics calculations. A fitted displacement field was then reconstructed by solving a minimization problem. More precisely, the quadratic distance between the experimental displacement field and the fitted displacement field was minimized under the constraint that forces are restricted to the cell surface and edges of the imaged area (using a penalty on forces in the minimization problem infinitesimal on the surfaces and very large in the matrix, such as 10^{-9} and 10^{-9} relative to the penalty on the displacement fit, for appropriately adimensionalized displacements and forces). A smoothing parameter was also included in the minimization to favor continuity of the forces. Using the fitted displacement field, all nine components of the stress tensor were computed on every position of the cubic mesh. The shear modulus experimentally measured for the fibrin + 10% Matrigel matrix (70 Pa) was used for these calculations. The stress tensor on the cell surface was then interpolated between these discrete positions using a Gaussian weighted average. The surface of the cell was finally meshed, which provided the normal vector on every point of the cell surface, and the normal pressure on this mesh was defined as $[\text{normal vector}]^t \times [\text{stress tensor}] \times [\text{normal vector}]$, and displayed as a color-code in the final figure.

Cultures of FACS Isolated Stem Cells: Lgr5-GFP and wild type mouse small intestinal organoids cultured in medium supplemented with valproic acid (VPA) and CHIR99021 (for stem cell enrichment as described by Yin et al.[42]) were collected. Matrigel was removed by washing twice in ice-cold Advanced DMEM/F12, followed by 7 min digestion with TrypLE. The cell suspensions were filtered through a 40 µm mesh. Cells were stained with 4′,6-diamidino-2-phenylindole (DAPI) shortly before acquisition. Fluorescence-activated cell-sorting (FACS) was performed using FACS Aria III (BD, Franklin Lakes, NJ, USA). DAPI negative, GFP positive cells were collected, pelleted by centrifugation, and resuspended in fibrin 3 mg mL^{-1} + laminin 2 mg mL^{-1} gels for plating and culturing as described previously.

PEG-Maleimide+RGD Hydrogels: The gels were formed with the protocols of Cruz-Acuña et al.,[23] using identical reagents and suppliers.

Gene Expression: Gene expression was quantified from human pancreas and liver organoids cultured in Matrigel or in fibrin 3 mg mL^{-1} + laminin 2 mg mL^{-1}. HEK cells were used as a control. For each condition, four hydrogels of 20 µL (or 500 000 HEK cells) were collected, and pelleted by centrifugation at 2000 g for 1.5 min. After removing the excess media, samples were frozen at −80 °C until use. After addition of lysis buffer, samples were homogenized by repeated pipetting and RNA was isolated using NucleoSpin miRNA kit (Macherey–Nagel) following manufacturer's instructions. The RNA concentration was determined with a plate reader (Synergy H1, BioTek Instruments). RNA with an absorbance ratio at 260/280 nm between 1.9 and 2.1 was used for quantitative polymerase chain reaction (qPCR) analysis. The Fast SYBR Green Master Mix (Applied Biosystems) was used to perform the PCR amplification with 150×10^{-9} M forward and reverse primer. Data were analyzed using the $2^{-\Delta\Delta Ct}$ method and normalized against the house-keeping gene GAPDH and the HEK controls.

Organoid Drug Assay using Defined Hydrogels: Human wildtype pancreas and PDAC organoid lines were dissociated and seeded in four replicates in 5 µL drops of hydrogels (Matrigel; 3 mg mL^{-1} fibrin + 10% Matrigel; 3 mg mL^{-1} fibrin + 2 mg mL^{-1} laminin) in 96 well black plates with clear bottom (Corning). Plates were incubated for 10 min in 37 °C and 5% CO_2 cell culture incubator to allow solidification of the gels. The hydrogel droplets were then overlaid with 100 µL of complete organoid media containing either DMSO 0.1%, Gemcitabine 1×10^{-6} M (Selleckchem) or Paclitaxel 1×10^{-6} M (Selleckchem). 72 h post seeding pictures were taken with a Zeiss Apotome, and Cell Titer Glo 3D measurements (Promega) were performed according to manufacture instructions. Luminescence readings were acquired with the Synergy H1 reader (BioTek).

Statistical Analysis: Statistically significant differences in colony formation efficiency/colony area/drug responses were assessed by a one-way analysis of variance (ANOVA) test followed by a Sidak's post-hoc test in Graphpad Prism 7.02 when the ANOVA p-value is under 0.05. p-values under 0.05 were considered significant. The annotations on graphs are: ns = not significant, * = $p < 0.05$, ** = $p < 0.01$, *** = $p < 0.001$, **** = $p < 0.0001$. When only two conditions were present, Student's t-tests were used. p-values from repeated measures ANOVA were used to compare the overall gene expression in Matrigel versus Fibrin/Laminin.

Supporting Information

Supporting Information is available from the Wiley Online Library or from the author.

Acknowledgements

N.B. and L.I. contributed equally to this work. The authors thank the Scientific Center for Optical and Electron Microscopy (ScopeM) of ETH Zurich for their support in imaging. This work was funded by the SNSF (31003A_160230). T.R. holds a PhD scholarship from the ETH.

Conflict of Interest

The authors declare no conflict of interest.

Keywords

fibrin, hydrogels, organoids

Received: March 13, 2018
Revised: June 11, 2018
Published online: September 10, 2018

[1] H. Clevers, *Cell* **2016**, *165*, 1586.
[2] G. Vlachogiannis, S. Hedayat, A. Vatsiou, Y. Jamin, J. Fernández-Mateos, K. Khan, A. Lampis, K. Eason, I. Huntingford, R. Burke, M. Rata, D.-M. Koh, N. Tunariu, D. Collins, S. Hulkki-Wilson, C. Ragulan, I. Spiteri, S. Y. Moorcraft, I. Chau, S. Rao, D. Watkins, N. Fotiadis, M. Bali, M. Darvish-Damavandi, H. Lote, Z. Eltahir, E. C. Smyth, R. Begum, P. A. Clarke, J. C. Hahne, M. Dowsett, J. de Bono, P. Workman, A. Sadanandam, M. Fassan, O. J. Sansom, S. Eccles, N. Starling, C. Braconi, A. Sottoriva, S. P. Robinson, D. Cunningham, N. Valeri, *Science* **2018**, *359*, 920.
[3] N. Sachs, J. de Ligt, O. Kopper, E. Gogola, G. Bounova, F. Weeber, A. V. Balgobind, K. Wind, A. Gracanin, H. Begthel, J. Korving, R. van Boxtel, A. A. Duarte, D. Lelieveld, A. van Hoeck, R. F. Ernst, F. Blokzijl, I. J. Nijman, M. Hoogstraat, M. van de Ven, D. A. Egan, V. Zinzalla, J. Moll, S. F. Boj, E. E. Voest, L. Wessels, P. J. van Diest, S. Rottenberg, R. G. J. Vries, E. Cuppen, H. Clevers, *Cell* **2018**, *172*, 373.e10.
[4] M. Schutte, T. Risch, N. Abdavi-Azar, K. Boehnke, D. Schumacher, M. Keil, R. Yildiriman, C. Jandrasits, T. Borodina, V. Amstislavskiy, C. L. Worth, C. Schweiger, S. Liebs, M. Lange, H.-J. Warnatz, L. M. Butcher, J. E. Barrett, M. Sultan, C. Wierling, N. Golob-Schwarzl, S. Lax, S. Uranitsch, M. Becker, Y. Welte, J. L. Regan, M. Silvestrov, I. Kehler, A. Fusi, T. Kessler, R. Herwig, U. Landegren, D. Wienke, M. Nilsson, J. A. Velasco, P. Garin-Chesa, C. Reinhard, S. Beck, R. Schäfer, C. R. A. Regenbrecht, D. Henderson, B. Lange, J. Haybaeck, U. Keilholz, J. Hoffmann, H. Lehrach, M.-L. Yaspo, *Nat. Commun.* **2017**, *8*, 14262.
[5] M. van de Wetering, H. Francies, J. Francis, G. Bounova, F. Iorio, A. Pronk, W. van Houdt, J. van Gorp, A. Taylor-Weiner, L. Kester, A. McLaren-Douglas, J. Blokker, S. Jaksani, S. Bartfeld, R. Volckman, P. van Sluis, V. Li, S. Seepo, C. Sekhar Pedamallu, K. Cibulskis, S. Carter, A. McKenna, M. Lawrence, L. Lichtenstein, C. Stewart, J. Koster, R. Versteeg, A. van Oudenaarden, J. Saez-Rodriguez, R. Vries, G. Getz, L. Wessels, M. Stratton, U. McDermott, M. Meyerson, M. Garnett, H. Clevers, *Cell* **2015**, *161*, 933.
[6] L. Broutier, G. Mastrogiovanni, M. M. Verstegen, H. E. Francies, L. M. Gavarró, C. R. Bradshaw, G. E. Allen, R. Arnes-Benito, O. Sidorova, M. P. Gaspersz, N. Georgakopoulos, B.-K. Koo, S. Dietmann, S. E. Davies, R. K. Praseedom, R. Lieshout, J. N. M. IJzermans, S. J. Wigmore, K. Saeb-Parsy, M. J. Garnett, L. J. van der Laan, M. Huch, *Nat. Med.* **2017**, *23*, 1424.
[7] R. J. Mills, D. M. Titmarsh, X. Koenig, B. L. Parker, J. G. Ryall, G. A. Quaife-Ryan, H. K. Voges, M. P. Hodson, C. Ferguson, L. Drowley, A. T. Plowright, E. J. Needham, Q.-D. Wang, P. Gregorevic, M. Xin, W. G. Thomas, R. G. Parton, L. K. Nielsen, B. S. Launikonis, D. E. James, D. A. Elliott, E. R. Porrello, J. E. Hudson, *Proc. Natl. Acad. Sci. USA* **2017**, *114*, E8372.
[8] G. Schwank, B.-K. Koo, V. Sasselli, J. Dekkers, I. Heo, T. Demircan, N. Sasaki, S. Boymans, E. Cuppen, C. van der Ent, E. Nieuwenhuis, J. Beekman, H. Clevers, *Cell Stem Cell* **2013**, *13*, 653.

[9] T. Nakamura, T. Sato, *Cell. Mol. Gastroenterol. Hepatol.* **2018**, *5*, 51.
[10] T. Sato, R. G. Vries, H. J. Snippert, M. van de Wetering, N. Barker, D. E. Stange, J. H. van Es, A. Abo, P. Kujala, P. J. Peters, H. Clevers, *Nature* **2009**, *459*, 262.
[11] D. Grün, A. Lyubimova, L. Kester, K. Wiebrands, O. Basak, N. Sasaki, H. Clevers, A. van Oudenaarden, *Nature* **2015**, *525*, 251.
[12] M. Huch, B.-K. Koo, *Development* **2015**, *142*, 3113.
[13] J. R. Spence, C. N. Mayhew, S. A. Rankin, M. F. Kuhar, J. E. Vallance, K. Tolle, E. E. Hoskins, V. V. Kalinichenko, S. I. Wells, A. M. Zorn, N. F. Shroyer, J. M. Wells, *Nature* **2011**, *470*, 105.
[14] T. Nakano, S. Ando, N. Takata, M. Kawada, K. Muguruma, K. Sekiguchi, K. Saito, S. Yonemura, M. Eiraku, Y. Sasai, *Cell Stem Cell* **2012**, *10*, 771.
[15] M. A. Lancaster, M. Renner, C.-A. Martin, D. Wenzel, L. S. Bicknell, M. E. Hurles, T. Homfray, J. M. Penninger, A. P. Jackson, J. A. Knoblich, *Cell Stem Cell* **2008**, *3*, 519.
[16] M. Eiraku, K. Watanabe, M. Matsuo-Takasaki, M. Kawada, S. Yonemura, M. Matsumura, T. Wataya, A. Nishiyama, K. Muguruma, Y. Sasai, *Cell Stem Cell* **2008**, *3*, 519.
[17] M. A. Lancaster, J. A. Knoblich, *Proteomics* **2010**, *10*, 1886.
[18] C. S. Hughes, L. M. Postovit, G. a. Lajoie, *Proteomics* **2010**, *10*, 1886.
[19] S. Vukicevic, H. K. Kleinman, F. P. Luyten, A. B. Roberts, N. S. Roche, A. Reddi, *Exp. Cell Res.* **1992**, *202*, 1.
[20] H. K. Kleinman, G. R. Martin, *Semin. Cancer Biol.* **2005**, *15*, 378.
[21] D. Seliktar, *Science* **2012**, *336*, 1124.
[22] N. Gjorevski, N. Sachs, A. Manfrin, S. Giger, M. E. Bragina, P. Ordóñez-Morán, H. Clevers, M. P. Lutolf, *Nature* **2016**, *539*, 560.
[23] R. Cruz-Acuña, M. Quirós, A. E. Farkas, P. H. Dedhia, S. Huang, D. Siuda, V. García-Hernández, A. J. Miller, J. R. Spence, A. Nusrat, A. J. García, *Nat. Cell Biol.* **2017**, *19*, 1326.
[24] M. Ehrbar, S. C. Rizzi, R. Hlushchuk, V. Djonov, A. H. Zisch, J. A. Hubbell, F. E. Weber, M. P. Lutolf, *Biomaterials* **2007**, *28*, 3856.
[25] N. Broguiere, L. Isenmann, M. Zenobi-Wong, *Biomaterials* **2016**, *99*, 47.
[26] G. Palazzolo, N. Broguiere, O. Cenciarelli, H. Dermutz, M. Zenobi-Wong, *Tissue Eng., Part A* **2015**, *21*, 2177.
[27] W. D. Spotnitz, *World J. Surg.* **2010**, *34*, 632.
[28] H. Nagase, G. B. Fields, *Biopolymers* **1996**, *40*, 339.
[29] M. P. Lutolf, J. L. Lauer-Fields, H. G. Schmoekel, A. T. Metters, F. E. Weber, G. B. Fields, J. A. Hubbell, *Proc. Natl. Acad. Sci. USA* **2003**, *100*, 5413.
[30] E. Öztürk, Ø. Arlov, S. Aksel, L. Li, D. M. Ornitz, G. Skjak-Braek, M. Zenobi-Wong, *Adv. Funct. Mater.* **2016**, *26*, 3649.
[31] J. Zhu, L. Liang, Y. Jiao, L. Liu, *PLoS One* **2015**, *10*, 1.
[32] M. Z bczyk, M. Blombäck, J. Majewski, G. Karkowski, H. N. Wallen, A. Undas, S. He, *Thromb. Haemostasis* **2015**, *113*, 851.
[33] G. Raeber, M. Lutolf, J. Hubbell, *Biophys. J.* **2005**, *89*, 1374.
[34] J. F. Dekkers, C. L. Wiegerinck, H. R. de Jonge, I. Bronsveld, H. M. Janssens, K. M. de Winter-de Groot, A. M. Brandsma, N. W. M. de Jong, M. J. C. Bijvelds, B. J. Scholte, E. E. S. Nieuwenhuis, S. van den Brink, H. Clevers, C. K. van der Ent, S. Middendorp, J. M. Beekman, *Nat. Med.* **2013**, *19*, 939.
[35] I. Todorov, K. Omori, M. Pascual, J. Rawson, I. Nair, L. Valiente, T. Vuong, T. Matsuda, C. Orr, K. Ferreri, C. V. Smith, F. Kandeel, Y. Mullen, *Pancreas* **2006**, *32*, 130.
[36] S. E. Sakiyama, J. C. Schense, J. A. Hubbell, *FASEB J.* **1999**, *13*, 2214.
[37] J. C. Schense, J. Bloch, P. Aebischer, J. A. Hubbell, *Nat. Biotechnol.* **2000**, *18*, 415.
[38] M. van de Wetering, H. Francies, J. Francis, G. Bounova, F. Iorio, A. Pronk, W. van Houdt, J. van Gorp, A. Taylor-Weiner, L. Kester, A. McLaren-Douglas, J. Blokker, S. Jaksani, S. Bartfeld, R. Volckman, P. van Sluis, V. Li, S. Seepo, C. Sekhar Pedamallu, K. Cibulskis, S. Carter, A. McKenna, M. Lawrence, L. Lichtenstein, C. Stewart, J. Koster, R. Versteeg, A. van Oudenaarden, J. Saez-Rodriguez, R. Vries, G. Getz, L. Wessels, M. Stratton, U. McDermott, M. Meyerson, M. Garnett, H. Clevers, *Cell* **2015**, *161*, 933.
[39] L. Broutier, A. Andersson-Rolf, C. J. Hindley, S. F. Boj, H. Clevers, B.-K. Koo, M. Huch, *Nat. Protoc.* **2016**, *11*, 1724.
[40] J. C. Schense, J. A. Hubbell, *Bioconjug. Chem.* **1999**, *10*, 75.
[41] R. F. Doolittle, K. W. K. Watt, B. A. Cottrell, D. D. Strong, M. Riley, *Nature* **1979**, *280*, 464.
[42] X. Yin, H. F. Farin, J. H. van Es, H. Clevers, R. Langer, J. M. Karp, *Nat. Methods* **2014**, *11*, 106.